Geomagnetic and Solar dependency of *MSTIDs* occurrence rate: A climatology based on airglow observations from the Arecibo Observatory Remote Optical Facility (ROF)

Pedrina Terra[1], Fabio Vargas[2], Christiano G. M. Brum[1] and Ethan S. Miller[3]

[1] University of Central Florida/ Arecibo Observatory, Puerto Rico, USA.

[2] University of Illinois at Urbana-Champaign, Illinois, USA.

[3] Johns Hopkins University Applied Physics Laboratory, Laurel, Maryland, USA; Now with Systems and Technology Research, Beavercreek, Ohio, USA.

Corresponding author: Pedrina Terra (pedrina.santos@ucf.edu)

Key Points:

- *MSTIDs* occurrence rate is modulated by solar activity, presenting periods of correlation and anti-correlation depending on the season.
- Even small increases in Kp index implies an increase of *MSTIDs* occurrence rate.
- The dependencies on these geophysical parameters are related to the thermospheric neutral winds behavior over Puerto Rico.

Abstract

We employ in this work the first *O(^{1}D) 630.0-nm* airglow dataset registered at the Remote Optical Facility (ROF) in Culebra, Puerto Rico, during the descending phase of the solar cycle #24. From November 4, 2015, to September 26, 2019, observations were carried out during 633 nights at ROF using a small all-sky imager, while *MSTID* events were identified in 225 of 499 nights classified as clear. A quantitative analysis of these *MSTIDs* and their dependency by geophysical parameters (solar and geomagnetic activities) are the main focus of this study. We introduce an original statistical methodology that examines the unique features of the dataset and minimizes the cross-contamination of individual modulators onto one another, avoiding bias in the results. Our findings include a primary peak of *MSTIDs* occurrence in the December solstice and a secondary peak in the June solstice. We observed a remarkable correlation in the occurrence rate of the *MSTIDs* with the geomagnetic activity. A notable modulation of the *MSTIDs* occurrence rate with the solar activity is also found, which includes periods of correlation and anti-correlation depending on the season. This modulation has an annual component that is ~33% and ~83% stronger than the semi-annual and terannual components, respectively. We discuss these findings based on the behavior of the thermospheric neutral winds derived from 30 years of Fabry-Perot interferometer observations. Our results, which are valid for low to moderate solar activity, point out circumstances that might explain differences in previous climatological studies of nighttime *MSTIDs.*

Plain Language Summary

The medium scale traveling ionospheric disturbances *(MSTID*s) are one of the most observed perturbations in the nighttime ionosphere in mid latitudes. Arguably, many aspects of their nature are still poorly understood. This paper focuses on a quantitative analysis of the *MSTIDs* observed at the Arecibo Observatory Remote Optical Facility (ROF) located in Culebra, Puerto Rico, using airglow images of the red line emission (630.00-nm). We show the occurrence rate of the *MSTIDs* found at ROF and their dependency on solar and geomagnetic activities. We discuss our findings based on the relation between the *MSTIDs* and the behavior of the background thermospheric neutral winds over Puerto Rico.

1 Introduction

Traveling Ionospheric Disturbances (*TIDs*) are fluctuations in the electron density and altitude of the ionospheric plasma that can occur in all latitudes. These fluctuations are thought to be an ionospheric manifestation of atmospheric gravity waves generated at high latitude and/or propagated from the lower atmosphere (Otsuka et al., 2013). The first observations of the *TIDs* dated from the 1950s (Munro, 1950; Price, 1953) using radio techniques. Later, it was observed that *TIDs* could propagate in a broad spectral range of speeds, scales and, periods (Georges, 1968; Francis, 1974). Those with a typical scale between 100km and 1000km were classified as medium-scale (*MSTIDs*) and those larger than 1000km as large-scale (*LSTIDs*) (Hunsucker et al., 1982).

MSTIDs can occur in the daytime and nighttime, and their source mechanisms can be different (e. g. Kotake et al., 2006; Makela and Otsuka, 2012). Hines (1960) was the first to suggest the atmospheric gravity waves as the cause of the irregular motions in the ionosphere. Hooke (1968) extended this theory by showing that the gravity waves propagating into the thermosphere affected the ionospheric plasma through collisions or recombination/production rate changes under the influence of the geomagnetic field. While the daytime *MSTIDs*

propagation agrees with the gravity waves seeding theory, the geometry for the direction of propagation and for the alignment of the nighttime *MSTIDs* generate many doubts about this source mechanism, opening discussions about the role of the Perkins instability (Perkins, 1973) in the generation of these nighttime events (Behnke, 1979; Miller et al., 1997; Shiokawa et al. 2003b). But further studies demonstrated that the growth rate of the Perkins mechanism was not enough to explain the evolution of the nighttime *MSTID*s (e. g., Garcia et al., 2000; Kelley et al., 2002). Besides that, the nighttime *MSTIDs* drift in a direction contrary to the plasma background (Narayanan et al., 2014). Numerical simulations pointed out that the electrodynamics involved in the coupling between the *E*- and *F*- ionospheric regions could resolve the discrepancies observed in the Perkins instability theory and reproduce the generation and proper direction of propagation of nighttime *MSTIDs* (Tsunoda and Cosgrove, 2001; Otsuka et al., 2007). Different types of structures in the *E* region were considered in this coupling theory as the quasiperiodic echoes, unstable sporadic *E* layers (*Es*), *Es* layer instability and just the presence of *Es* layers (Martinis et al., 2019). On other hand, Otsuka et al. (2013) suggested that the longitudinal and seasonal *MSTIDs* occurrence on Europe was not controlled by the *Es* layer occurrence alone.

Climatological studies of the nighttime *MSTID*s, including their features and geophysical modulators (solar and geomagnetic activities), have been carried out in several locations around the globe, attempting to elucidate the possible sources and evolution of these events that are still poorly understood. The seasonal occurrence of the nighttime *MSTIDs* was found to have a semi-annual behavior in the Japanese sector with a primary peak in summer (June solstice) and the secondary peak in winter (December solstice) (Shiokawa et al. 2003a). In the North American sector, Martinis et al. (2010) also observed a semi-annual behavior in the occurrence of these events but with a primary peak in December solstice and a secondary one in June solstice. Duly et al. (2013) observed large number of occurrences of nighttime *MSTIDs* during the solstices in Central Pacific and South American. In the Brazilian sector, a peak of occurrence of nighttime *MSTIDs* near the June solstice months was reported by various studies (e. g., Figueiredo et al., 2018; Pimenta et al., 2008; Paulino et al., 2016). Some authors studied the *MSTIDs* occurrence from two or more locations and concluded that it varies with the longitude (e. g., Kotake et al., 2006; Tsuchiaya et al., 2019).

An anti-correlation of the nighttime *MSTIDs* occurrence on the solar activity was observed in various studies (e. g., Amorim et al., 2011; Duly et al., 2013; Garcia et al., 2000; Martinis et al., 2010; Narayanan et al., 2014; Shiokawa et al., 2003a). Nonetheless, Fukushima et al. (2012) reported a decrease in the *MSTIDs* occurrence as the result of a decrease in the solar activity, while Fedorenko et al. (2013) using numerical simulations, claimed that *MSTIDs* occurrence does not depend on solar activity.

Studies relating the occurrence of the *MSTID*s with the geomagnetic activity are also controversial. For instance, Seker et al. (2011) suggested a negative correlation between the occurrence of *MSTIDs* and the geomagnetic activity by analyzing optical data registered at Arecibo Observatory (AO). Burke et al. (2016), stated that *MSTIDs* manifest no apparent dependence on geomagnetic activity variation. Paulino et al. (2016) reported that the geomagnetic activity was not an essential factor for the occurrence modulation of *MSTIDs* at low latitude stations. Frissel et al. (2016) also found no correlation between the geomagnetic activity and occurrence of *MSTIDs* observed with SuperDARN. Conversely, Chen et al. (2019) found that under different geomagnetic conditions, the occurrence rate of the *MSTID*s presented some variation, i.e., an increase of the occurrence rate with the rise of the geomagnetic activity.

In this scenario of several studies describing distinct dependencies of the *MSTIDs* occurrence on the solar and geomagnetic activities, it is clear that more details about their climatology and modulators needed to be investigated. Nevertheless, rather than more experiments, a crucial factor is how to improve the usual statistical methodologies to understand this phenomenon better. The literature shows that the classic methods, which are usually based on pre-established thresholds or average values for the classification of solar and geomagnetic activities, result in a non-optimal sample, even when the database consists of years of observations. Also, these methods do not minimize the cross-contamination of individual modulators onto one another, generating bias in the results. We propose a statistical methodology that maximizes the unique features of the data distribution according to the parameters to be investigated. This unusual method allowed us to extract what we believe is the closest to the real scenario of the variability of nighttime *MSTIDs* occurrence with equivalent samples for the different geophysical conditions and season, resulting in more reliable results.

This work focuses on the nighttime *MSTIDs* observed at the Arecibo Observatory Remote Optical Facility (ROF) during the descending phase of the solar cycle #24. Note that in the remainder of this paper, the term "*MSTIDs"* refers to nighttime *MSTIDs*. While this paper is focused on the quantitative (occurrence) analysis of the *MSTID* events observed at ROF over almost four years of observation, a complete qualitative analysis of these events will be presented and discussed in a separate work.

2 The Arecibo Observatory Remote Optical Facility (ROF)

The *O(^{1}D) 630.0-nm* airglow emission images used in this work are the first set of optical data collected at ROF, located in Culebra, a small island in the east of Puerto Rico's archipelago (approximately 150 km from AO). Culebra is a federal nature reserve and was chosen due to its geographical and climatological characteristics, as well as the low light contamination, making it a strategic site for optical experiments. The main goal of establishing the ROF was to add new resources to the observing optical capability of AO by increasing the statistics of observations under optimal sky conditions, and also by adding a new geometry for the study of the wave structures propagating in the mesosphere and low thermosphere (MLT) region.

Initially, the ROF was deployed in an area of 340 m^2 at the central portion of Culebra (18^{o}19'03" N; 65^{o}16'40" W). One climate-controlled container was placed on this site hosting the optical and radio receiver instrumentation. The ROF operated continuously from November 4, 2015, to September 4, 2017. Due to the slow recovery following hurricanes Irma and Maria in Puerto Rico (September 5 and 20, 2017, respectively) and subsequent re-competition of the cooperative agreement for the management of the Arecibo Observatory, the ROF was temporarily disassembled. Finally, on May 27, 2018, an updated ROF resumed operations in a more secluded location in Culebra, under the new management of the University of Central Florida (UCF). Since then, the ROF is in continuous operation and expanding its cluster of optical and radio instrumentation.

At present, the ROF occupies an area of 500 m^2 at the north coast of Culebra (18^{o}19'47" N; 65^{o}18'25" W). There are two climate-controlled containers on site: one hosts optical and radio instruments and a control room; the other is lodging for scientists and technicians. One of the relevant features of the updated ROF is its sustainability: a solar system with backup feeds the facility, and the water collected from the rain is kept in a reservoir for use. This feature is particularly crucial for maintaining operations during the Atlantic Hurricane Season. Figure 1

shows the two locations of ROF (actual-ROF_2 and former-ROF_1 sites) as well as some features of the facility.

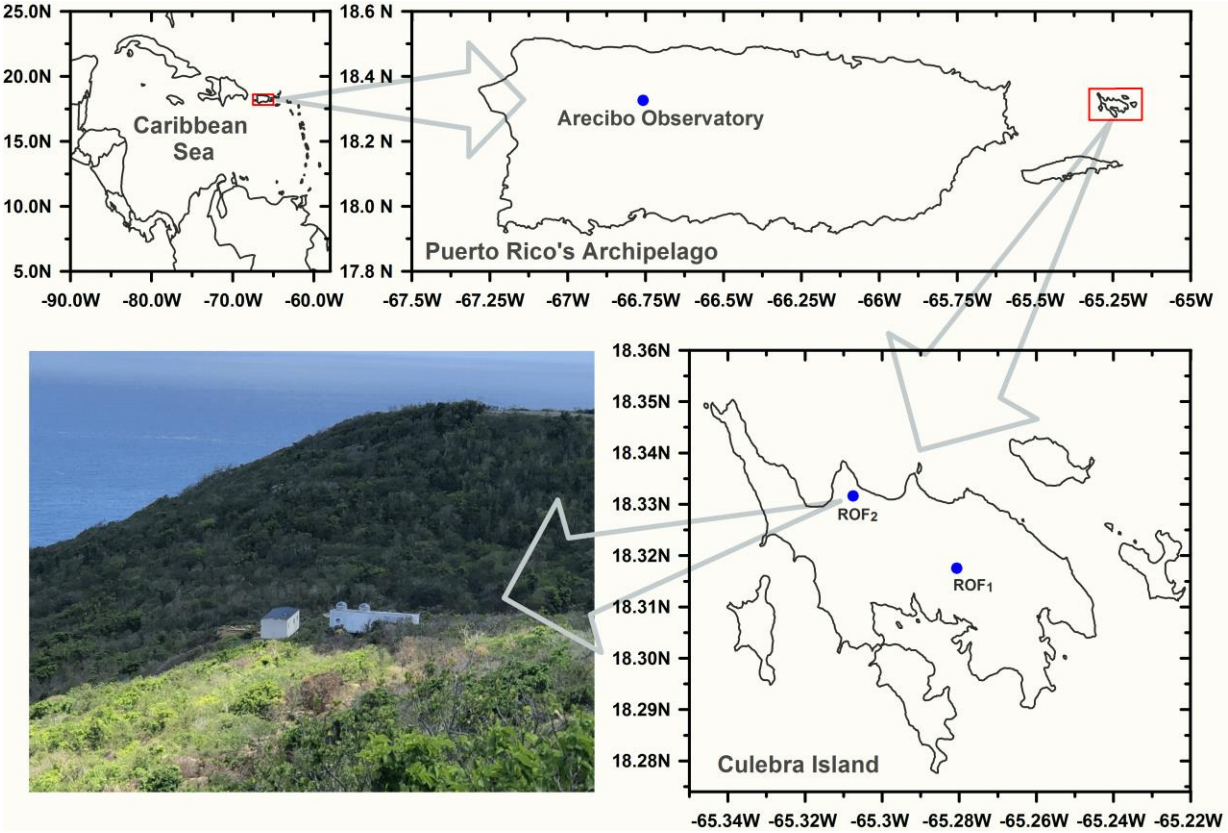

Figure 1. The Arecibo Observatory Remote Optical Facility (ROF) location to the Caribbean Sea/Puerto Rico sector. The ROF_2 and ROF_1 denote the current and previous locations of ROF, respectively. The container with the domes on top in the left bottom pane hosts the optical and radio instrumentation and a control room, while the other is lodging for scientists and technicians.

3 Instrumentation and Airglow Data

Mendillo et al. (1997) were the pioneers in detecting *MSTIDs* using all-sky imagers to observe the thermospheric *OI 630.0-nm* airglow emission. Since then, this optical technique has been widely used to obtain two-dimensional images of these events in the upper atmosphere (e. g. Amorim et al., 2011, Duly et al., 2013; Garcia et al., 2000; Martinis et al., 2010; Pimenta et al., 2008; Seker et al., 2011; Sivakandan et al., 2019).

A two-step process produces the *630.0-nm* airglow emission: *i)* a neutral-ion charge exchange reaction where the neutral oxygen molecules (O_2) are ionized by the ions of oxygen atoms (O^+), and *ii)* the dissociative recombination of O_2^+ that produces excited atomic oxygen at the ^1D level. When the excited oxygen atomic $O(^1D)$ decays to the ground state (^3P), a photon with a wavelength of *630.0-nm* is emitted. The concentration of O^+ is higher around ~300 km of altitude and the O_2^+ concentration decrease with height due to the atom/molecule mass diffusion. As a consequence, the *630.0-nm* airglow emission peak occurs in the bottom of the ionospheric *F*-layer (around 250-280 km), being a very sensitive indicator of *F*-layer height and density

variations. The fluctuations of the ionospheric plasma in this layer caused by the presence of *MSTID*s are observed in the *630.0-nm* airglow images as bright and dark bands that can occur individually or as multiple structures.

The *OI 630.0-nm* airglow emission data used in this work were acquired with a Walden Small all-sky imager, which is a relatively low-cost, small all-sky fisheye spectral imager with an Atik 314L+ detector and a charge-coupled device (CCD) chip of 1392x1040 pixels. The five-position filter wheel holds narrow bandpass 2-inch interference filters. Observations of the atmospheric airglow emissions in a given sequence throughout the night can be adjusted depending on the desired wavelength emission. The small all-sky imager was built by the Computational Physics, Inc - CPI New England (formerly known as Scientific Solutions, Inc. or SSI). The manufacturer also provides the Imagetool Control software. More details about this system is found at https://www.cpi.com/spectral.html#imagers.

For this study, two filters that record oxygen emissions from the thermospheric *OI 630.0-nm* emission and from the off-band *OI 643.4-nm* were used. Two minutes of exposure time was used for each filter, except during campaigns. We removed the background and dark count frames from the images, which were then treated to find an optimal contrast level, allowing a better visual inspection of the data and detection of the *MSTID* events. As the images were taken with a fisheye-type lens, an unwrapping procedure was applied to correct lens distortions. This unwrapping procedure maps the field of view onto a 512x512 pixel grid with resolution of 2 km/pixel, shifts the image in x and y directions to bring the zenith pixel to the center of the image, and rotates the array to align the geographic north of the field of view to the top of the frame (mapped images retain ~120 degrees of the original field-of-view).

Figure 2 show a *MSTID* observed at ROF on July 04, 2016 (top left panel). The image shows the Northwestward (NW) wave front of the *MSTID* traveling Southwestward (SW). At the top right panel is the image from the *O(^{1}S) 643.4-nm* used to remove the background from the previous image. The bottom panels show the resulting mapping procedure for the images shown on the top panels. Notice how the fisheye lens effect distorts the *MSTID* wave front across the field-of-view.

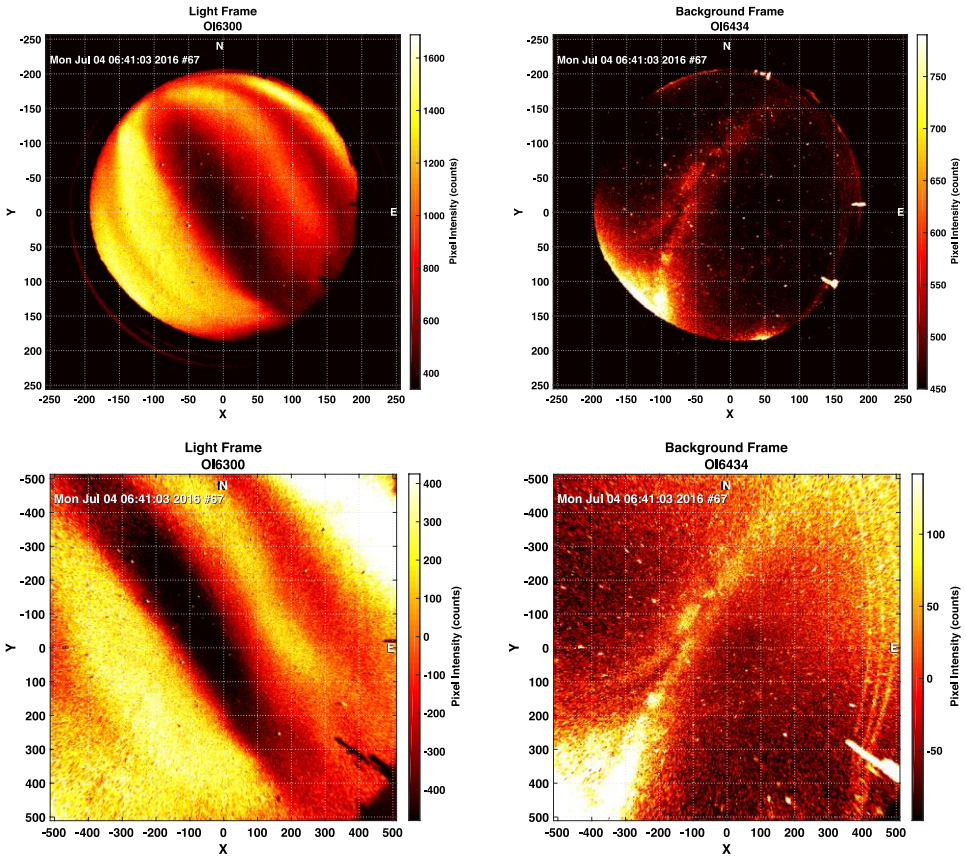

Figure 2. The left top panel shows an example of a *MSTID* observed on the OI 630.00-nm airglow emission at ROF on July 04, 2016, at 06:41:03 UT using a Walden Small All-Sky Imager. The exposition time was 240s. Note the Northwest - Southeast alignment. The right top panel shows the image from *OI 643.4-nm* airglow used to remove the background removed from the image on the left. The bottom panels are images shown on the top panels mapped in a 512x512 pixel grid with a resolution of 2 km/pixel.

4 Methodology and Analyses

A total of 633 nights of observations were registered from November 4, 2015, to September 26, 2019, with 78.83% of them (499 nights) considered as “clear nights”. Our criteria for a clear night was a sequence of at least 3 hours of relative cloud-free sky. This percentage of clear skies found at ROF shows an improvement of the optical capability, in comparison to previous studies using airglow emissions from the AO. For example, in Garcia et al. (2000) analysis of images from January 5, 1997, to April 10, 1998, approximately 61% of their database were considered clear nights. However, they labeled “clear nights” as nights with at least 1.5 hours of clear-sky condition (this is half of the time considered in our statistics). Martinis et al. (2010) also presented a detailed statistical distribution of clear nights at AO. They observed the *630.0-nm* airglow emission during 942 nights for approximately 5-years (from 2002 to 2007). Clear nights were found in 57.96% (546 nights) of the period. Their criterion was 3 hours or more of good weather conditions allowing for the viewing of the background airglow. In summary, ROF presented 33% or more clear skies than these previous studies using data from AO.

The signatures of the *MSTID*s in the *OI 630.0-nm* airglow emission were observed in 225 nights (45.09% of the total clear nights) of our dataset. Figure 3 (top and middle panels) shows the distribution of the clear nights and the nights with *MSTID* events, respectively, according to the day of the year (DOY). The entire database (499 nights) was divided into bins of 28 days for optimal sampling (represented by the bar chart), and also by season which is represented by the blue line, and encompasses about 92 nights around the solstices and the equinoxes (the center of the seasons is indicated below the DOY axis in blue). It is observed that the clear nights at ROF are highly dependent on season (top panel of Figure 3), presenting a large annual variation, with a maximum in June solstice (local summer, 155 nights) and the minimum during the September equinox (~55% fewer occurrences, 85 nights). The appearance of clear skies for the March equinox seems to be only the smooth transition of the number of clear skies from the winter to summer. The same feature is not seen for the September equinox, which is way smaller, probably due to the hurricane season in the Atlantic North and Caribbean regions, which peaks around the August-September months.

The occurrence rate of the *MSTID*s is shown at the bottom panel of Figure 3, as well as the seasonal dependence of the *MSTID*s detected at AO in previous studies by Seker et al. (2011), Martinis et al. (2010) and Garcia et al. (2000), which are represented by green crosses, black dots and magenta arrows, respectively. Seker et al. (2011) used image data from 2003 to 2007, with F10.7cm (F10.7) SFU (Solar Flux Unit, 1 SFU = 10^{-22}W/m^2/Hz) varying from ~148 to ~80 SFU; Martinis et al. (2010) analyses were based on image data from 2002 to 2007 and F107 varying from ~150 to ~80 SFU; and Garcia et al. (2000) observations were from January 1997 to February 1998 with F10.7 varying from ~60 to ~110 SFU.

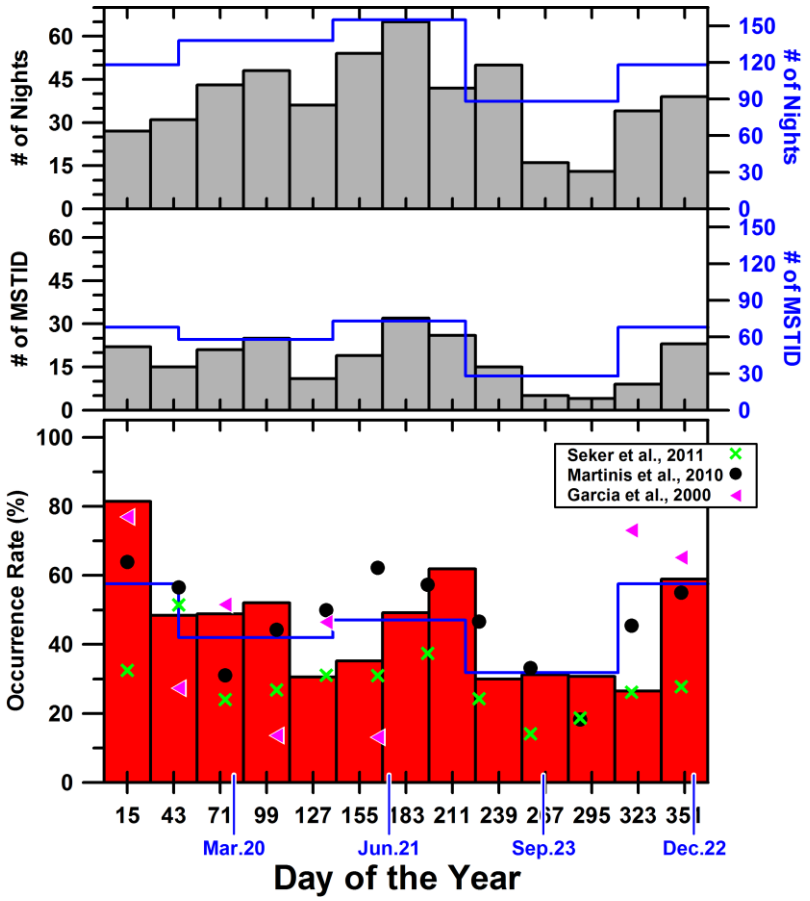

Figure 3. The top and middle panel shows the distribution of 499 clear nights and *MSTID* events according to the day of the year, respectively. In all the panels, the bar chart corresponds to 28 days bins of data. The bottom panel shows the occurrence rate of *MSTIDs* found at ROF. The monthly occurrence of *MSTIDs* registered at AO by Seker et al. (2011) is represented by the green crosses, ones found by Martinis et al. (2010) is represented by the black dots, and the ones found by Garcia et al. (2000) by magenta arrows, which are shown here for comparison. The blue line in all panels represent the distribution of clear nights and *MSTID* events by season. The center of the seasons is indicated by the abscissa in blue.

The main point of the methodology introduced here is to analyze the occurrence of *MSTIDs* based on the unique features of our dataset. Therefore, the identification of the variability of the solar and geomagnetic activities in our data is a key point in this work. Figure 4 shows these variabilities quantified by the F10.7 and Kp indexes, respectively. In the left top panel, the dots represent the clear nights. The red dots indicate the nights with *MSTID* events, while the blue dots represent the nights were *MSTID*s were not detected. The right top panel shows the occurrence rate of our dataset for different levels of F10.7. It is observed that most of the data were registered during low solar condition (F10.7< ~80 SFU), and some were detected during moderate activity (80 SFU < F10.7 <110 SFU). Another important feature observed in the top panels of Figure 4 is that even though the dataset was registered during the descending phase of the solar cycle #24, there is a period (from 2015 to 2017) with a large variability of F10.7 when compared to the period encompassing the years of 2018 and 2019. This particular feature needs to be taken into consideration when investigating the modulation of the *MSTIDs*

occurrence rate by the geomagnetic activity. *Why?* Lower F10.7 variability in the sample analyzed implies less cross-contamination of the solar activity dependency into the geomagnetic activity modulation of the *MSTIDs* occurrence, avoiding bias in the results. Therefore, the analysis regarding the geomagnetic activity need to be time restricted to the period where the F10.7 is virtually constant (from June 2, 2018 to September 26, 2019), as shown in the left bottom panel of Figure 4. The occurrence rate of the Kp level in this period is presented on the right panel of Figure 4. It is observed that most of the data was acquired during low geomagnetic activity ($Kp<=3^0$), and very few samples during moderate to disturbed geomagnetic activity ($3^0<Kp<=5^0$). Such Kp distribution is expected, as discussed by Wrenn et al. (1987).

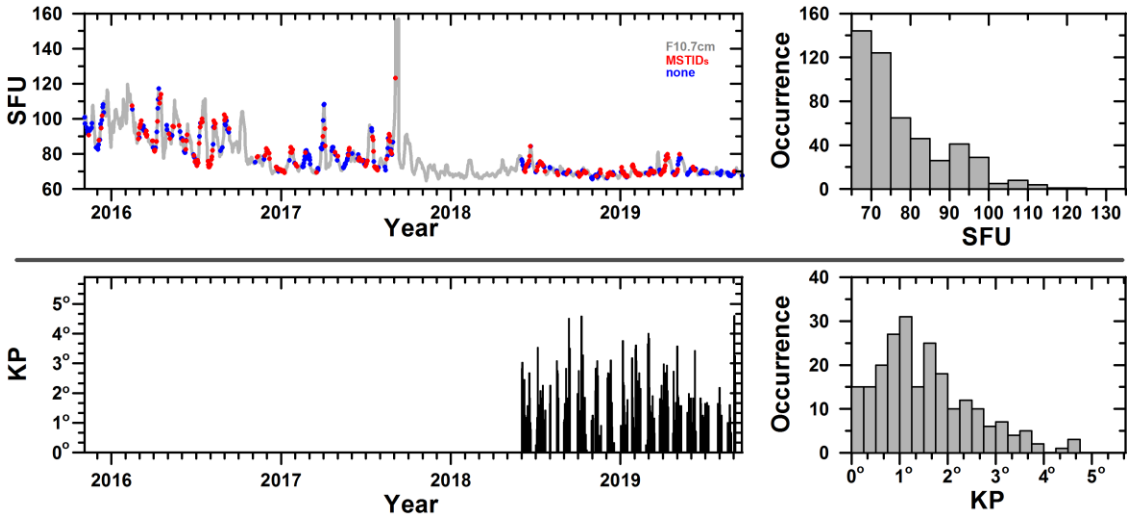

Figure 4. Variability of the solar and geomagnetic activity (quantified by the F107 and the Kp indexes, respectively) found in our data. In the left top panel, the dots represent the clear nights, the red dots being the nights with *MSTID* events, and the blue dots represent the nights that *MSTID*s were not detected. The right top panel shows the occurrence rate of our data regarding the F107 activity. The left bottom panel shows the time restricted period used on the geomagnetic dependence analysis. The right bottom panel shows the occurrence rate of the Kp levels found on our data for this period.

The features presented in Figure 4 were carefully considered and were the base for defining the samples in our analysis. No pre-established thresholds or monthly averages for the solar and geomagnetic activities were used, avoiding any masking trend on the results. We also minimized the well-defined seasonal dependency of the *MSTIDs* occurrence previously showed in Figure 3 during the investigation of the modulation by the geophysical parameters.

In Figure 5, the dataset was divided into blocks of two subsequent months to guarantee a more reliable investigation regarding the modulator being studied (in this case the solar activity). Six of the twelve groups analyzed are shown in the top panel of Figure 5 (the intermediary groups were not shown for better visualization). The letters on each plot refer to the initials of months used in that group (i.e., D-J means December and January and so on). The dots represent the *MSTIDs* occurrence rate by the averaged F10.7 of the clear skies for each group in a specific year. The numbers close to the dots are the number of nights used in each average, and the horizontal lines represent the standard deviation of the F10.7 variability in those periods. The red line in each plot is the best linear fitting for that group and shows the dependence of the occurrence rate of the *MSTIDs* in respect to F10.7.

The bottom panel in Figure 5 shows the slopes (occurrence rate of the *MSTID*s by SFU) of the fittings for the 12 groups analyzed (open circles). Through a Fast Fourier Transform (*FFT*) following the procedure of Brum et al. (2011) and Brum et al. (2012), the occurrence rate of the *MSTID*s by SFU along the year was decomposed in three harmonics (more significant periodicities), which are shown by the blue (first harmonic m=1, 12 months), orange (second harmonic m=2, 6 months), and green (third harmonic m=3, 4 months) lines . The grey line represents the re-constructed curve from these harmonics.

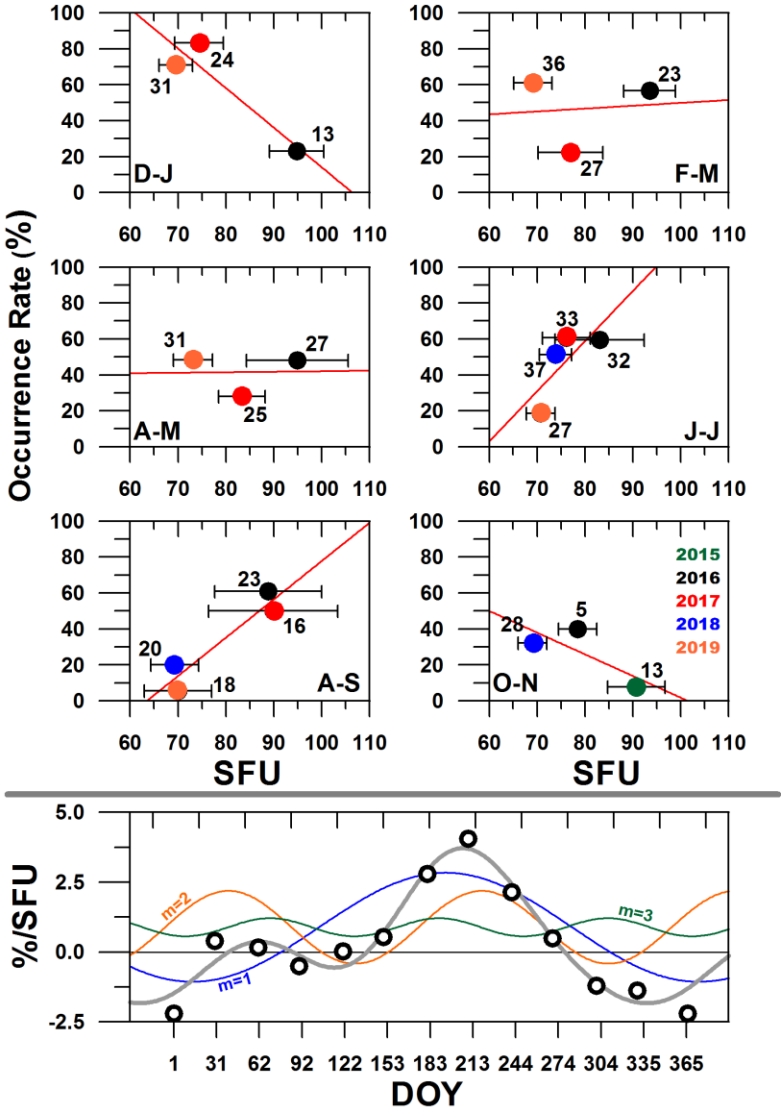

Figure 5. Responses of the *MSTID*s occurrence to the solar activity variability. The six blocks on the top panel shows the *MSTID*s occurrence rate per periods of two months in function of F107 and its respective best linear approximation. The bottom panel shows the *MSTIDs* occurrence rate by the solar decimetric flux (%SFU^{-1}, black dots) in function of day of the year along with the three main periodicities (most relevant ones obtained by FFT). The light grey line represents the FFT reconstruction based on the three harmonics: blue line is the first harmonic (m=1); orange line represents the second harmonic (m=2); and the green line is the third harmonic (m=3).

As described previously, only the data acquired from June 2, 2018 to September 26, 2019 are used to investigate the dependency of the *MSTIDs* occurrence rate by the geomagnetic activity. The effects of the seasonality are minimized by distributing the data into three seasons: December solstice, equinoxes and, June solstice. Both equinoxes were merged to provide similar amount of days (samples) than the solstices. Therefore, each season encompasses about 4 months of observation. We assumed the Kp index as the average of the 6 hours before and 3 hours during the *MSTID* events. To guarantee an optimal statistical sampling for each season, our dataset was sorted out from the lowest to the highest Kp values and subsequently divided into four sections with the same percentage of samples for each range of Kp (25% each) (upper panel of Figure 6). The average of the F10.7 (open circles) and its variability (vertical bar) for each section is also presented on the top panel to show that the methodology adopted (minimize the solar activity trends) allowed an optimal sampling with very little variations on the F10.7. The bottom panel of Figure 6 shows the occurrence rate of the *MSTIDs* according to Kp for each section of the seasons. The open circles represent the average of Kp for a percentage of nights that *MSTID*s were detected in each section of the top panel, and the horizontal lines are their variability (standard deviation). The numbers next to the circles represent the total nights used in the average. The best linear fitting is also shown for each season (blue lines), as well as the slope (SLP) or occurrence rate in respect to the geomagnetic activity variation (%Kp^{-1}) and the correlation factor (R).

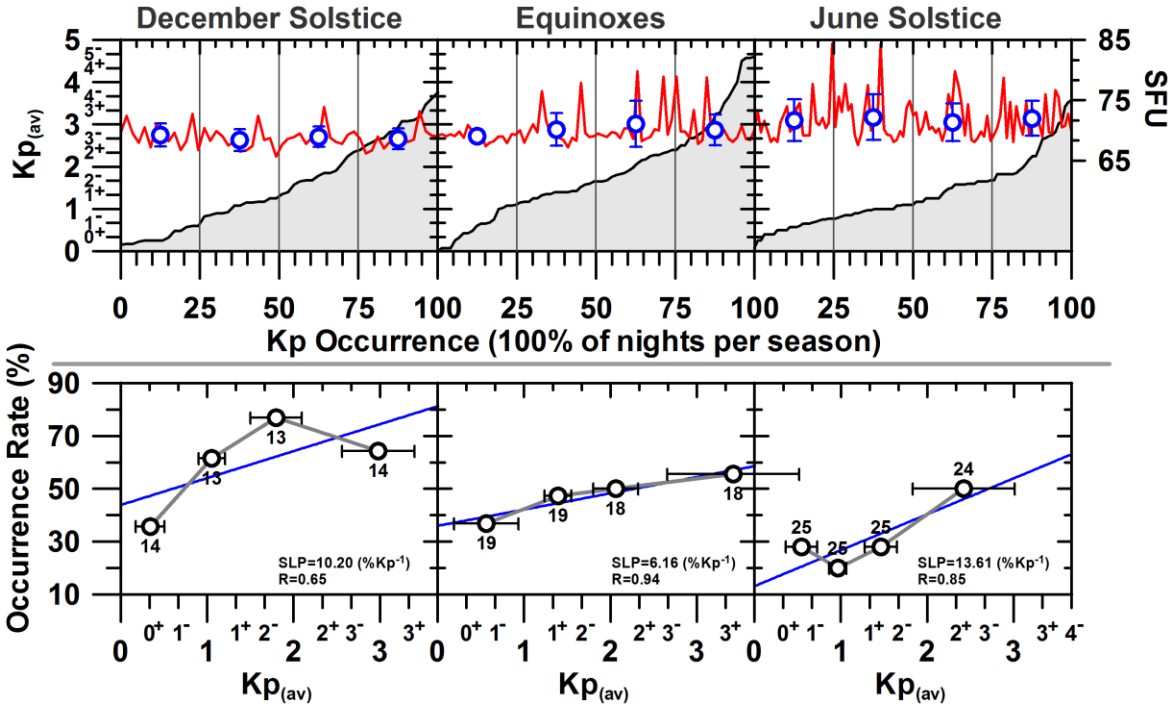

Figure 6. Responses of the *MSTIDs* occurrence rate to the variation on the geomagnetic activity. The distribution of clear nights per season is presented in the upper panel sorted by the geomagnetic activity condition. Notice that each season was divided into four sections of same amount of nights containing different levels of geomagnetic activity. The bottom panels show the occurrence rate of *MSTID*s by the Kp average of each one of the sections shown in the upper panels. The slope (variability of the occurrence rate by geomagnetic activity, %Kp^{-1}) and the correlation index obtained by linear regression is also presented as well.

5 Discussions

The discussions presented in this paper are focused on the quantitative analysis of the *MSTIDs* occurrence rate detected at ROF along the studied period, being valid for low to moderate solar activity (F10.7 cm Solar Flux ranging from ~65 to ~125 SFU). Although this quantitative analysis does not allow for the investigation of the source of these *MSTIDs*, it does result in a detailed climatology of these events that enable the evaluation of their geophysical modulators.

Our findings are discussed based on the characteristics of the background thermospheric neutral winds over Puerto Rico. These winds play a direct role in the dynamics of the ionosphere-thermosphere system, being an indicator of the background conditions that are more favorable for the generation and/or development (growth) of the *MSTIDs* by the Perkins instability. Even though this instability by itself does not explain the observed features of the *MSTIDs*, it has an essential role in the *MSTIDs* occurrence theories. For example, Yokoyama et al. (2009) and Yokoyama and Hysell (2010) have developed a three-dimensional numerical model that simulates the *MSTIDs* by the coupling processes between the *E*- and *F*- regions at midlatitudes. They concluded that an *Es* layer instability plays a major role in the generation of the *MSTIDs* in the F- region, and the Perkins instability is required to amplify the initial its perturbation. Kelley (2011) presented the theory that *MSTIDs* originate in the auroral zone as gravity waves. The waves traveling in the preferred Perkins orientation could reach the midlatitudes where the *E*- and *F*- region coupling effect amplifies *MSTID* structures observed in the O(^1D) nightglow.

At AO (and ROF) latitudes (both locations are expected to have the same dynamics due to proximity), the eastward component of the thermospheric neutral winds can destabilize the equilibrium of the ionospheric *F*-layer and trigger the Perkins instability, while the southward component is responsible to stabilize this system (Kelley, 2011). The growth rate of this instability depends on the physics controlled by these two winds components, and on the unstable $\boldsymbol{k}$-vector of the wave. The growth rate maximizes when the eastward component of the thermospheric neutral winds is dominant and the $\boldsymbol{k}$-vector is at either in the NE of SW quadrants (Garcia et al., 2000). *MSTIDs* propagating in those quadrants will draw energy from the global ionospheric current system, the source of energy for the Perkins process, and grow in amplitude (Kelley and Miller, 1997).

In our discussions we use detailed studies of the behavior and features of the thermospheric neutral winds presented by Brum et al. (2011), which were based on 30 years of Fabry-Perot interferometers observations at AO. These winds at Puerto Rico are mainly modulated by season (Brum et al., 2011; Tepley et al., 2011) and their response to the solar and geomagnetic activities have a substantial seasonal and local time dependence (Brum et al., 2011).

5.1 Seasonal dependence of the *MSTIDs* occurrence rate

We observed a clear semi-annual distribution of the *MSTIDs* occurrence rate at ROF, with a primary peak in December solstice (local winter) and a secondary peak in June solstice (local summer), as shown in the bottom panel of Figure 3. Similar behavior was observed by Martinis et al. (2010*)* and Seker et al. (2011) in previous studies using airglow data from AO. Garcia et al. (2000*)* also observed a peak in December solstice over AO but they had no available data for June solstice. These results are also shown on the bottom panel of Figure 3. Some

differences between the percentage of the occurrence rate found by these previous studies and our analysis are noted. Our results showed a higher peak on December solstice, which is in agreement with that found by Garcia et al. (2000). On the other hand, Martinis et al. (2010) and Seker et al. (2011) had found lower percentage of the occurrence rate peak during the December solstice. For June solstice the situation reverses, and the occurrence rate from our results is smaller than those observed by Martinis et al. (2010) and Seker et al. (2011). We will return to the discussion about these differences in Section 3.2.

Martinis et al. (2010*)* attributed the semi-annual seasonal behavior of the *MSTIDs* to the coupling between the *E*- and *F*- layers and to the inter-hemispheric coupling, while Seker et al. (2011) tried to associate it with the seasonal variation of geomagnetic activity finding no correlation between them. Studies from other locations suggested that the *Es* layer plasma density may control the season variations of the nighttime *MSTIDs* occurrence rates (e. g., Otsuka et al., 2007; Park et al., 2010; Saito et al., 2007). A more recent study by Otsuka et al. (2013) suggested that besides the strong *E* region activity, other factors should be involved in the growth of the instabilities in order to explain the local winter peak in the European sector observed by them. Although all these mechanisms are feasible, we emphasize the importance of the background conditions of the neutral atmosphere and its influence on our results.

The Figures 5a and 5b of Brum et al. (2012) shows the seasonal residual behavior of the zonal and meridional components of the thermospheric neutral winds respectively, obtained by the subtraction of the data value minus the yearly average under the same solar conditions for a given hour. They found that on average, these winds are more to the NE quadrant during the local winter (December solstice) and more to the SW quadrant during the local summer (June solstice). During the equinoxes these winds are transiting from one quadrant to another. This seasonal behavior of the thermospheric neutral winds found by Brum et al. (2012) coincides with the semi-annual distribution of occurrence rate of the *MSTIDs* found in this work (bottom of Figure 3), which peaks on December solstice and June solstices. These results also corroborate with the theoretical analysis of the Perkins instability that predicts that the growth rate of the instability maximizes when the wave ***k***-vector is toward the NE or SW quadrants in the northern hemisphere (e. g. Garcia et al., 2000).

5.2 Solar activity control of the *MSTIDs* occurrence rate

From the analysis presented on the top panels of Figure 5, a clear modulation of the *MSTID*s occurrence by the F10.7 is observed, which is season dependent. During the December solstice (local winter), the occurrence rate of the *MSTID*s is anti-correlated with the F10.7. However, it is correlated during the June solstice (local summer). On March equinox, there is no significant modulation of the *MSTIDs* occurrence by the F10.7. The transition between the maximum and the minimum of the *MSTIDs* occurrence rate happens during September equinox. The bottom panel of Figure 5 shows that the annual component of this dependency is the primary modulator, presenting an amplitude of 1.95 $\%SFU^{-1}$, which is ~33% larger than semi-annual component that is 1.30 $\%SFU^{-1}$. The terannual component is less relevant, with amplitude of 0.32 $\%SFU^{-1}$. These notable features of the solar activity controlling the *MSTID*s occurrence rate might explain the difference in the amplitude of the occurrence rate found in this study and the ones from Martinis et al. (2010) and Seker et al. (2011) (presented in bottom panel of Figure 3). Although both studies were during the descending phase of solar activity, the previous solar cycle #23 had higher activity than the solar cycle #24. Therefore, the F10.7 values found on

Martinis et al. (2010) and Seker et al. (2011) database were higher than ours. For example, for December and June solstices Martinis et al. (2010) had the maximum value of F107 reaching 180 SFU, while the ones on our database reached a maximum of 110 SFU. By analyzing the bottom panel of Figure 5, we conclude that a higher (lower) F10.7 (as Martinis et al. (2010) and Seker et al. (2011) compared with our F10.7 range), produces a smaller (bigger) occurrence rate of *MSTID* in December (June) solstice. The F10.7 range of Garcia et al., (2000) database was very similar to ours for December solstice, which explains the close agreement of both results.

Several studies in different locations observed a negative correlation between the occurrence of *MSTIDs* and the solar activity (e.g. Shiokawa et al., 2013a; Takeo et al., 2017; Tshuchiya et al., 2019). They explained this negative correlation in terms of the linear growth rate of the Perkins instability, which is inversely proportional to the average ion-neutral collision frequency and the scale height of neutral atmosphere. On other hand, the ion-neutral collision frequency and the scale height of the neutral atmosphere are positively related with solar activity. Thus, the growth-rate of the Perkins instability is inversely proportional to solar activity. Vargas (2019) used another approach to explain this anti-correlation. Using a simulation model, he showed that it is due to the *O(^{1}D) 630.0-nm* airglow layer vertical structure, which benefits the observation of longer rather than shorter vertical wavelength *MSTIDs* during high solar activities. In other words, he found that as the airglow layer gets thicker as the solar activity increases, its response to shorter vertical wavelength waves is attenuated, and only longer vertical scale *MSTIDs* (less frequent events) will be detectable from the ground.

Our results show that for low-to-moderate solar activity (F10.7 ranging from ~65 to ~125 SFU), there is a component on the *MSTIDs* growth and/or occurrence that is able to control its modulation by the solar activity. Also, it was found that this component is seasonally dependent. As mentioned before, the background thermospheric neutral winds at Puerto Rico responds to the solar activity with a substantial seasonal and local time dependencies. This behavior is presented in Figure 7 of Brum et al. (2012). During the local winter (December solstice) the thermospheric neutral winds propagate more NW, changing to NE at summer (June solstice) and being in the transition between these two quadrants during equinoxes. Analyzing our results presented on Figure 5 and based on this behavior of the thermospheric neutral winds, the negative correlation between the *MSTIDs* occurrence and the F107 happens in December solstice when these winds are in the NW quadrant (not favorable to the Perkins instability), and the positive correlation happens during June solstice when the *TNW* are in the NE quadrant (favorable to the Perkins instability). During equinox our results do not show any significative modulation by the F107, which coincides with the transition of the thermospheric neutral winds between one quadrant to another.

5.3 Geomagnetic activity control of the *MSTIDs* occurrence rate

Figure 6 shows a positive correlation between the occurrence rate of the *MSTIDs* at ROF with the geomagnetic activity. Note that our dataset presents very few geomagnetic disturbed periods however, we found that even small increases in the Kp index implies an increase of the occurrence of *MSTIDs*. We believe that this result suggests that the interaction between the thermosphere and ionosphere has another component besides the variations of photoionization and recombination rates produced by gravity wave pressure fronts, indicating that the thermospheric neutral wind transport plasma along the geomagnetic field is a key factor in the occurrence of the *MSTIDs*.

Returning to the investigation of the background thermospheric neutral winds over Puerto Rico, the two top rows of Figure 10 from Brum et al. (2012) show that an increase in the geomagnetic activity (Kp index), under low solar activity conditions, will intensify these winds in the SW direction (favorable to the Perkins instability). This intensification is dependent on the season, being ~ 9 $ms^{-1}Kp^{-1}$ in December solstice, ~ 7-8 $ms^{-1}Kp^{-1}$ during the equinoxes and ~ 4-5 $ms^{-1}Kp^{-1}$ during the June solstice. Comparing this behavior with our results presented in bottom panel of Figure 6, the strongest modulation of the occurrence rate of the *MSTIDs* occur in June solstice followed by the December solstice. During the equinoxes this modulation is weaker than the other seasons.

6 Summary

We employed the first *O(^{1}D) 630.0-nm* airglow dataset registered at the Arecibo Observatory Remote Optical Facility (ROF) during the descending phase of the solar cycle #24. The establishment of the ROF in the island of Culebra accomplished with the expectation of providing new resources to the observing optical capability of the AO, increasing the statistics of observations. In summary, clear nights conditions were found in 78.83% of the observation period, representing 33% or more clear skies than previous studies using data from AO. The clear nights at ROF were found to be highly dependent on season, presenting a large annual variation, with a maximum in June solstice and the minimum during the September equinox.

Signatures of the *MSTID*s in the *OI 630.0-nm* airglow emission were observed in 225 nights (45.09% of the total clear nights). The purpose of this work was to investigate the occurrence of these *MSTID*s and its modulation by solar and magnetic activities. We introduced an original statistical methodology that allowed us to extract the variability of the *MSTIDs* occurrence with equivalent samples for the different geophysical conditions, based on the examination of the unique features of our dataset. This method also minimized the cross-contamination of individual modulators onto one another, avoiding bias in the results.

The occurrence rate of the *MSTID* events showed a clear semi-annual distribution with a primary peak in December solstice (local winter) and a secondary peak in June solstice (local summer). This climatology coincides with the thermospheric neutral winds behavior at Puerto Rico, which is more to the NE quadrant during the local winter (December solstice), more to the SW quadrant during the local summer (June solstice) and transient between these two quadrants during the equinoxes. Also, these results corroborate with the theoretical analysis of the Perkins instability that predicts that the ***k***-vector of the instability maximizes toward the NE or SW quadrants in the northern hemisphere.

We found a notable modulation of the *MSTIDs* occurrence rate with the solar activity. This modulation included periods of correlation and anti-correlation depending on the season, presenting an annual component that is ~33% and ~83% stronger than the semi-annual and terannual components, respectively. This result pointed out circumstances that might explain the differences in previous climatological studies of nighttime *MSTIDs* from AO. Our results show that the *MSTIDs* occurrence rate dependence on the solar activity seems to be controlled by the thermospheric neutral winds. The negative correlation between the *MSTIDs* occurrence rate and the F107 happens in December solstice when these winds are in the NW quadrant (not favorable to the Perkins instability), and the positive correlation happens during June solstice when the winds are in the NE quadrant (favorable to the Perkins instability). During equinox our results do

not show any significative modulation by the F107, which coincides with the transition of the thermospheric neutral winds between one quadrant to another.

A remarkable positive correlation between the *MSTIDs* occurrence rate and the geomagnetic activity was also found. We observed that even small increases in the Kp index implies an increase of the occurrence of *MSTIDs*. This result was interpreted as an indicator that the neutral wind transport plasma along the geomagnetic field is a key factor in the *MSTIDs* occurrence over ROF. Studies from the thermospheric neutral winds over Puerto Rico showed that an increase in the Kp index, under low solar activity conditions, intensify these winds in the SW direction (favorable to the Perkins instability). This intensification is dependent on the season, being ~ 9 $ms^{-1}Kp^{-1}$ in December solstice, ~ 7-8 $ms^{-1}Kp^{-1}$ during the equinoxes and ~ 4-5 $ms^{-1}Kp^{-1}$ during June solstice. Comparing this behavior with our results, the strongest modulation of the occurrence rate of the *MSTIDs* occur in June solstice followed by the December solstice. For the equinoxes, this modulation is weaker than the other seasons.

We emphasize that our results are valid for low to moderate solar activity (F10.7 cm ranging from ~65 to ~125 SFU). A complete qualitative analysis of these *MSTID* events observed at ROF is the focus of future work in progress.

Acknowledgments, and Data

- The Arecibo Observatory is a facility of the National Science Foundation operated under cooperative agreement by the University of Central Florida in alliance with Yang Enterprises, Inc., and Universidad Ana G. Méndez (UAGM).
- The Walden Small All-Sky Imager deployed at ROF was supported by the National Science Foundation (NSF) under AGS Grant #1463967 from PI: Ethan S. Miller.
- Fabio Vargas research has been supported by the National Science Foundation under 1. NSF AGS Grant #17-59573 and 2. NSF AGS Grant #19-03336.
- The imager data used in this study are publicly available and archived on the Arecibo Madrigal database website (http://naic.edu/madrigal).
- We thank Juanita Riccobono from CPI for the technical support.

References

Amorim, D. C. M.; Pimenta, A. A., Bittencourt, J. A., and Fagundes, P. R. (2011), Long-term study of medium-scale traveling ionospheric disturbances using OI 630 nm all-sky imaging and ionosonde over Brazilian low latitudes, J. Geophys. Res., 116, A06312, doi:10.1029/2010JA016090.

Behnke, R. (1979), F layer height bands in the nocturnal ionosphere over Arecibo, J. Geophys. Res., 84(A3), 974-978, doi: 10.1029/JA084iA03p00974.

Brum, C. G. M., Rodrigues, F. S., dos Santos P. T., Matta, A. C., Aponte, N., Gonzalez S. A., and Robles, E. (2011), A modeling study of foF2 and hmF2 parameters measured by the Arecibo incoherent scatter radar and comparison with IRI model predictions for solar cycles 21, 22, and 23, J. Geophys. Res.,116, A03324, doi:10.1029/2010JA015727.

Brum, C. G. M., Tepley, C. A., Fentzke, J. T., Robles, E., dos Santos, P. T., and Gonzalez, S. A. (2012), Long-term changes in the thermospheric neutral winds over Arecibo:

569 Climatology based on over three decades of Fabry-Perot observations, J. Geophys.
570 Res.,117, A00H14, doi:10.1029/2011JA016458.

571 Burke, W. J., Martinis, C. R., Lai, P. C., Gentile, L. C., Sullivan, C., and Pfaff, R. F. (2016),
572 C/NOFS observations of electromagnetic coupling between magnetically conjugate
573 MSTID structures, J. Geophys. Res. Space Physics, 121, 2569-2582,
574 doi:10.1002/2015ja021965.

575 Chen, G., Zhou, C., Liu, Y., Zhao, J., Tang, Q., Wang, X., and Zhao, Z. (2019), A statistical
576 analysis of medium-scale traveling ionospheric disturbances during 2014-2017 using the
577 Hong Kong CORS network, Earth Planets Space, 71(1), doi:10.1186/s40623-019-1031-9.

578 Duly, T. M., Chapagain, N. P., and Makela, J. J. (2013), Climatology of nighttime medium-scale
579 traveling ionospheric disturbances (MSTIDs) in the Central Pacific and South American
580 Sectors, Ann. Geophys., 31, 2229 – 2237, doi:10.5194/angeo-31-2229-2013.

581 Fedorenko, Y. P., Tyrnov, O. F., Fedorenko, V. N., and Dorohov, V. L. (2013), Model of
582 traveling ionospheric disturbances. J. Space Weather Space Clim., 3, A30,
583 Doi:10.1051/swsc/2013052.

584 Figueiredo, C. A. O. B., Takahashi, H., Wrasse, C. M., Otsuka, Y., Shiokawa, K., and Barros, D.
585 (2018), Investigation of Nighttime MSTIDS observed by Optical Thermosphere Imagers
586 at Low Latitudes: Morphology, Propagation Direction, and Wind Filtering, J. Geophys.
587 Res. Space Physics, 123, 7843-7857, doi:10.1029/2018ja025438.

588 Francis, S. H. (1974), A Theory of Medium-Scale Traveling Ionospheric Disturbances, J.
589 Geophys. Res., 79(34), 5245 – 5260, doi:10.1029/JA079i034p05245.

590 Frissel, N. A., Baker, J. B. H., Ruohoniemi, J. M., Greenwald, R. A., Gerrard, A. J., Miller, E. S.,
591 and West, M. L. (2016), Sources and characteristics of medium-scale traveling
592 ionospheric disturbances observed by high-frequency radars in the North American
593 sector, J. Geophys. Res. Space Physics, 121, 3722-3739, doi:10.1002/2015/JA022168.

594 Fukushima, D., Shiokawa, K., Otsuka, Y., and Ogawa, T. (2012), Observation of equatorial
595 nighttime medium-scale traveling ionospheric disturbances in 630-nm airglow images
596 over 7 years, J. Geophys. Res., 117, A10324, doi:10.1029/2012ja017758.

597 Garcia, F. J., Kelley, M. C., Makela, J. J., and Huang, C. -S. (2000), Airglow observation of
598 mesoscale low-velocity traveling ionospheric disturbances at midlatitudes, J. Geophys.
599 Res., 105(A8), 18407–18415, doi:10.1029/1999JA000305.

600 Georges, T. M. (1968), HF Doppler studies of traveling ionospheric disturbances, Journal of
601 Atmospheric and Terrestrial Physics, 30(5), 735 – 746, doi:10.1016/S0021-
602 9169(68)80029-7.

603 Hines, C. O. (1960), Internal Atmospheric Gravity Waves at Ionosphere Heights, Canadian
604 Journal of Physics, 38 (11), 1441-1481, doi:10.1139/p60-150.

605 Hooke, W. H. (1968), Ionospheric irregularities produced by internal atmospheric gravity waves,
606 J. Atmos. Terr. Phys., 30(5), 795-823, doi:10.1016/S0021-9169(68)80033-9.

607 Hunsucker, R. D. (1982), Atmospheric gravity waves generated in the high-latitude ionosphere:
608 A review. Rev. Geophys., 20(2), 293-315, doi:10.1029/RG020i002p00293.

609 Kelley, M. C. (2011), On the origin of mesoscale TIDs at midlatitudes, Ann. Geophys., 29, 361-
610 366, doi:10.5194/angeo-29-361-2011.

611 Kelley, M. C., Makela, J. J., and Saito, A. (2002), The mid-latitude F region at the mesoscale:
612 Some progress at last, J. Atmos. Terr. Phys., 64, 1525-1529, doi:10.1016/S1364-
613 6826(02)00090-1.

614 Kelley, M. C., and Miller, C. A. (1997), Electrodynamics of midlatitude spread F 3.
615 Electrohydrodynamic waves? A new look at the role of electric fields in thermospheric
616 wave dynamics, J. Geophys. Res. Space Physics, 102(A6), 11539 – 11547,
617 doi:10.1029/96ja03841.

618 Kotake, N., Otsuka, Y., Tsugawa, T., Ogawa, T., and Saito, A. (2006), Climatological study of
619 GPS total electron content variations caused by medium-scale traveling ionospheric
620 disturbances, J. Geophys. Res., 111, A04306, doi:10.1029/2005JA011418.

621 Makela, J. J., and Otsuka, Y. (2012), Overview of Nighttime Ionospheric Instabilities at Low
622 Latitude and Mid-Latitudes: Coupling Aspects Resulting in Structuring at the Mesoscale,
623 Space Sci. Rev. 168, 419-440, doi 10.1007/s11214-011-9816-6.

624 Martinis, C., Baumgardner, J., Wroten, J., and Mendillo, M. (2010), Seasonal dependence of
625 MSTIDs obtained from 630.0 nm airglow imaging at Arecibo, Geophys. Res. Lett., 37,
626 L1103, doi:10.1029/2010gl043569.

627 Mendillo, M., Baumgardner, J., Nottingham, D., Aarons, J., Reinisch, B., Scali, J., and Kelley,
628 M. (1997), Investigations of thermospheric-ionospheric dynamics with 630-Å images
629 from the Arecibo Observatory, J. Geophys. Res., 102 (A4), 7331-7343,
630 doi:10.1029/96ja02786.

631 Martinis, C., Yokoyama, T., and Nishioka, M. (2019), All-Sky Imaging Observations and
632 Modeling of Bright 630-nm Airglow Structures Associated With MSTIDs, J. Geophys.
633 Res. Space Physics, 124(8), 7332–7340. doi:10.1029/2019ja026935.

634 Miller, C. A., Swartz, W. E., Kelley, M. C., Mendillo, M., Nottingham, D., Scali, J., and
635 Reinisch, B. (1997), Electrodynamics of midlatitude spread *F*: 1. Observations of
636 unstable, gravity wave-induced ionospheric electric fields at tropical latitudes, J.
637 Geophys. Res., 102(A6), 11,521-11,532, doi: :10.1029/96JA03839.

638 Munro, G. H. (1950), Travelling disturbances in the ionosphere. Proc. R. Soc, Lond, A., 202,
639 208-223. Doi: 10.1098/ rspa. 1950.0095.

640 Narayanan L., V., Shiokawa, K., Otsuka, Y., & Saito, S. (2014), Airglow observations of
641 nighttime medium-scale traveling ionospheric disturbances from Yonaguni: Statistical
642 characteristics and low-latitude limit, J. Geophys. Res. Space Physics, 119(11), 9268–
643 9282, doi:10.1002/2014ja020368.

644 Otsuka, Y., Onoma, F., Shiokawa, K., Ogawa, T., Yamamoto, M., and Fukao, S. (2007),
645 Simultaneous observations of nighttime medium-scale traveling ionospheric disturbances
646 and E-region field-aligned irregularities at midlatitude, J. Geophys. Res., 112, A06317,
647 doi:10.1029/20055JA011548.

Otsuka, Y., Suzuki, K., Nakagawa, S., Nishioka, M., Shiokawa, K., and Tsugawa, T. (2013), GPS observations of medium-scale traveling ionospheric disturbances over Europe, Ann. Geophys., 31(2), 153-172, doi:10.5194/angeo-31-163-2013.

Park, J., Luhr, H., Min, K. W., and Lee, J. (2010), Plasma density undulations in the nighttime mid-latitude F-region as observed by CHAMP, KOMPSAT-1, and DMSP F15, J. Atmos. Terr. Phys., 72(2-3), 183-192, doi:10.1016/j.jastp.2009.11.007.

Paulino, I., Medeiros A. F., Vadas, S. L., Wrasse, C. M., Takahashi, H., Buriti, R. A., Leite, D. Filgueira, S., Bageston, J. V., Sobral, J. H. A., and Gobbi, D. (2016), Periodic waves in the lower thermosphere observed by OI 630 nm airglow images. Ann. Geophys., 34(2), 293-301, doi:10.5194/angeo-34-293-2016.

Perkins, F. (1973), Spread F and ionospheric currents, J. Geophys. Res., 78(1), 218-226, doi:10.1029/JA078i001p00218.

Pimenta, A. A., Kelley, M. C., Sahai, Y., Bittencourt, J. A., and Fagundes, P. R. (2008), Thermospheric dark bands structures observed in all-sky OI 630 nm emission images over the Brazilian low-latitude sector, J. Geophys. Res., 113, A01307, doi:10.1029/2007ja012444.

Price, R. (1953), Travelling disturbances in the Ionosphere. Nature, 115-115 doi:10.1038/172115b0

Saito, S., Yamamoto, M., Hashiguchi, H., Maegawa, A., and Saito, A. (2007), Observational evidence of coupling between quasi-periodic echoes and medium scale traveling ionospheric disturbances, Ann. Geophys., 25(10), 2185–2194, doi:10.5194/angeo-25-2185-2007.

Seker, I., Fung, S. F., and Mathews, J. D. (2011), Relation between magnetospheric state parameters and the occurrence of plasma depletion events in the nighttime midlatitude F region, J. Geophys. Res., 116(A4), doi:10.1029/2010ja015521.

Shiokawa, K., Ihara, C., and Ogawa, T. (2003a), Statistical study of nighttime medium-scale traveling ionospheric disturbances using midlatitude airglow images. J. Geophys. Res., 108(A1), 1052, doi:10.1029/2002ja009491.

Shiokawa, K., Otsuka Y., Ihara, C., Ogawa, T., and Rich, F. J. (2003b), Ground and satellite observations of nighttime medium-scale traveling ionospheric disturbance at midlatitude, J. Geophys. Res., 108(A4). doi:10.1029/2002ja009639.

Sivakandan, M., Chakrabarty, D., Ramkumar, T. K., Guharay, A., Taori, A., and Parihar, N. (2019), Evidence of Deep Ingression of Midlatitude MSTID into as low as ~3.5^0 Magnetic latitude, J. Geophys. Res. Space Physics, 124(1), 749-764, doi:10.1029/2018ja026103.

Takeo, D., Shiokawa, K., Fujinami, H., Otuska, Y., Matsuda, T. S., Ejiri, M. K., Nakamura, T., and Yamamoto. (2017), Sixteen year variation of horizontal phase velocity and propagation direction of mesospheric and thermosphere waves in airglow images at Shigaraki, Japan, J. Geophys. Res. Space Physics, 122, 8770-8780, doi:10.1002/2017JA023919.

Tepley, C., Robles, E., Garcia, R., Santos, P. T., Brum, C. M., and Burnside, R. G. (2011), Directional trends in thermosphere neutral winds observed at Arecibo during the past three solar cycles, J. Geophys. Res, 116, A00H06, doi:10.1029/2010JA016172.

Tsuchiya, A., Shiokawa, K., Fujinami, H., Otsuka, Y., Nakamura, T., Connors, M., Schofield, I., Shevtsov, B., and Poddelskiy, I. (2019), Three-dimensional Fourier analysis of the phase velocity distributions of mesospheric and ionospheric waves based on airglow images collected over 10 years: Comparison of Magadan, Russia, and Athabasca, Canada., J. Geophys. Res.: Space Physics, 124(10), 8110–8124, doi:10.1029/2019ja026783.

Tsunoda, R. T., & Cosgrove, R. B. (2001), Coupled electrodynamics in the nighttime midlatitude ionosphere, Geophys. Res. Lett., 28(22), 4171–4174, doi:10.1029/2001gl013245.

Vargas, F. (2019), Traveling Ionosphere Disturbance Signatures on Ground – Based Observation of the O(^{1}D) Nightglow Inferred from 1D Modeling, J. Geophys. Res. Space Physics, 124(11), 9348–9363. doi:10.1029/2019ja027356.

Wrenn, G. l., Rodger, A.S., and Rishbeth H. (1987), Geomagnetic storms in the Antarctic F-region. I. Diurnal and seasonal patterns for main phase effects, J. Atmos. Terr. Phys., 49, 9, 901-913. doi:10.1016/0021-9169(87)90004-3.

Yokoyama, T., and Hysell, D. L. (2010), A new midlatitude ionosphere electrodynamics coupling model (MIECO): latitudinal dependence and propagation of medium scale traveling ionospheric disturbances, Geophys. Res. Lett. 37(8), L08105, doi:10.1029/2010GL042598.

Yokoyama, T., Hysell, D. L., Otsuka, Y., and Yamamoto, M. (2009), Three-dimensional simulation of the coupled Perkins and Es-layer instabilities in the nighttime midlatitude ionosphere, J. Geophys. Res. Space Physics, 114(A3), doi:10.1029/2008ja013789.